

Strong Intermolecular Electronic Coupling of Chromophores Confined in Hydrogen-Bonded Frameworks

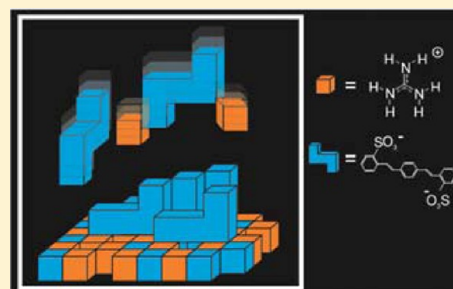
Published as part of the *Crystal Growth & Design* Margaret C. (Peggy) Etter Memorial virtual special issue

Takuji Adachi, David M. Connors, Wenchang Xiao, Chunhua Hu, and Michael D. Ward*

Department of Chemistry and Molecular Design Institute, New York University, 100 Washington Square East, New York, New York 10003-6688, United States

S Supporting Information

ABSTRACT: Guanidinium organodisulfonate (GDS) hydrogen-bonded frameworks constructed from “tetris-shaped” ortho-substituted disulfonated stilbene derivatives display crystal architectures in which the stilbenes serve as pillars that connect opposing guanidinium sulfonate (GS) sheets in a continuously layered architecture while guiding the organization of the stilbene residues into packing motifs that produce unique optical properties. The constraints imposed by ortho-substitution result in a heretofore unreported topology of the pillars projecting from the two-dimensional GS sheet, while the dense packing of stilbene constituents, confined between the GS sheets, results in strong intermolecular electronic coupling. Stilbene 420 (2,2''-([1,1'-biphenyl]-4,4'-diyl)di-2,1-ethenediyl)bis-benzenesulfonate) pillars pack in a face-to-face brickwork motif, producing a large bathochromic shift (~100 nm) of the absorbance and emission spectra relative to stilbene 420 in methanol. The distyrylbenzenedisulfonate (2,2'-((1E,1'E)-1,4-phenylenebis(ethene-2,1-diyl))dibenzenesulfonate) pillars, which pack in a face-to-face herringbone motif between the GS sheets, afford both hypsochromic and bathochromic shifts in their absorption spectrum, indicative of an unusually large Davydov splitting. The observation of both bathochromic and hypsochromic shifts can be attributed to the herringbone arrangement, in which both transitions are allowed due to the nonzero vector sum of the transition dipoles in both states. The large magnitude of the Davydov splitting reflects the strong intermolecular coupling between the chromophores, enforced by confinement in the GS framework. The newly discovered GS architectures evoke a new design rule that permits prediction of GS topologies in the case of longer tetris-shaped pillars.



INTRODUCTION

The prediction of molecular packing in the solid state based on the chemical structure of a molecule remains challenging because the energy difference between possible structures can be very subtle due to complex accumulation of weak forces. Even the most minute modifications in the chemical structure of a crystal constituent can alter the molecular packing significantly.^{1,2} One approach to the rational design of molecular packing in crystalline solids invokes the use of directional hydrogen bonding to dominate other weak intermolecular forces. Many advances relying on this approach have built on the pioneering work of Margaret “Peggy” Etter, who taught the solid-state chemistry community about the rules for hydrogen bonding patterns in organic solids from graph sets³ to the role of hydrogen bond donor–acceptor rankings as a determinant in solid-state structure.⁴ Peggy described the hydrogen bond as “like the attraction of a hummingbird to a flower—strong and directional, and also, lovely,” a quote that adorns the cover of a special issue in *Chemistry of Materials* in 1994 that was dedicated to Peggy and her accomplishments.⁵ Her role in the proliferation of hydrogen bonding as a tool for the design of crystalline organic solids and the field of “crystal engineering” is indisputable.

Not all hydrogen bonds in molecular crystals are alike, displaying a wide range of donor–acceptor combinations as well as hydrogen bond strengths. Charge-assisted hydrogen bonds are especially potent with respect to their structure directing ability, as the ionic charge reinforces the electrostatic nature of the hydrogen bond.^{6–9} For example, (guanidinium)N–H···O(carboxylate) hydrogen bonds or (hexamine metal)N–H···O(sulfonate)^{10–13} have proven to be useful for the assembly of crystalline networks. One of the most prolific series of molecular crystals is based on charge-assisted (guanidinium)N–H···O(sulfonate) hydrogen bonds, evolving from two inaugural publications coauthored by Etter and Ward in 1994,^{14,15} two years after her untimely death. Victoria Russell, a graduate student coauthor, began her thesis with Peggy but completed it with Ward in 1995. These early manuscripts spawned an expansive collection of compounds based on an unusually persistent two-dimensional (2D) guanidinium sulfonate (GS) network, which usually adopts a quasi-hexagonal symmetry owing to complementary 3-fold

Received: April 1, 2015

Revised: May 22, 2015

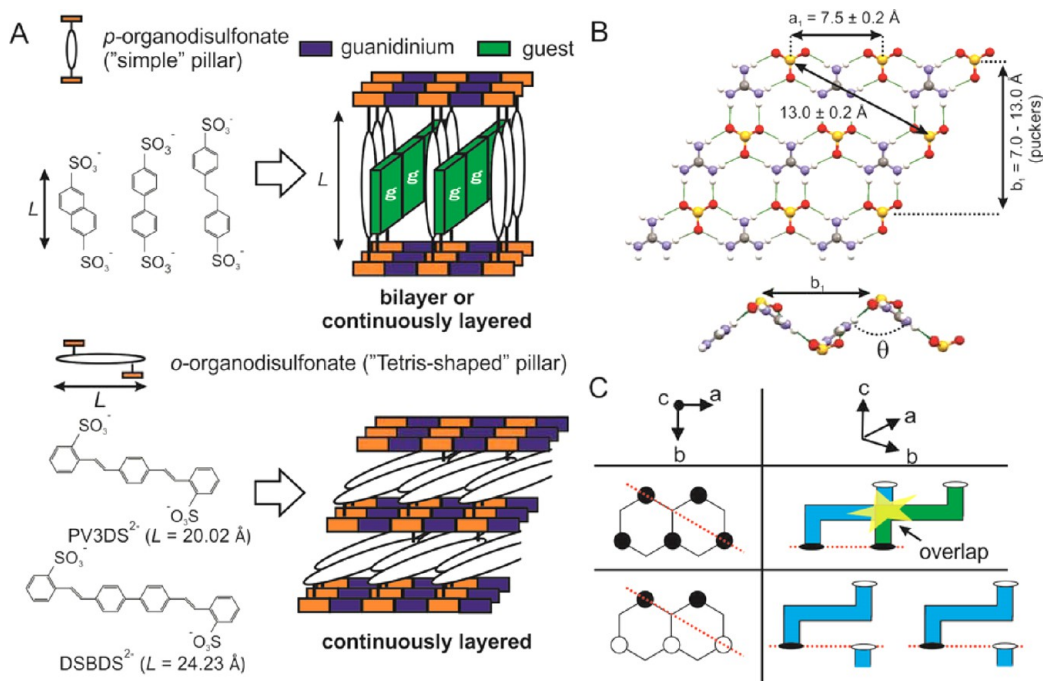


Figure 1. (A) Comparison of the known and anticipated architectures for para-substituted “pillars” and ortho-substituted organodisulfonate “tetris-shaped pillars”. The former align with their long axis nominally perpendicular to the GS sheets, creating cavities that are occupied by guest molecules, whereas the long axis of the tetris-shaped pillars would be expected to align parallel to the GS sheets, eliminating void space required for guest inclusion. The length of pillars L accounts for van der Waals radii. (B) Structure of a typical quasi-hexagonal GS sheet illustrating key distances between sulfonate nodes. θ is the puckering angle. (C) Schematic representation of the top-view (left) and side-view (right) representation of GS sheet. Filled and open circles represent “up” and “down” projections of the sulfonate nodes, respectively. The red dashed lines represent possible orientations of the long axis of the tetris-shaped pillars on the flat GS sheet. Unlike para-substituted pillars, the “all up” configuration, in which both sulfonate groups are connected to the same sheet, is prohibited for tetris-shaped pillars due to the strict requirement for commensurism between the sulfonate–sulfonate distance in the pillar and sulfonate nodes on a single GS sheet. This requirement is relaxed for the continuously layered architecture, which allows a long tetris-shaped pillar to traverse a void region created by a sulfonate node in a “down” projection.

symmetry and hydrogen bond donors and acceptors. The pendant organic substituents attached to the sulfonate moiety project from the GS network, serving as pillars (for disulfonates with sulfonate groups on opposite ends) or posts (for monosulfonates) that support lamellar stacking as well as inclusion cavities between the sheets.^{16–18} The resilience of the GS network to such a wide range of pillars and guests (in the case of inclusion compounds) can be attributed to the strength of the charge-assisted hydrogen bonds and a unique structural compliance through puckering of the GS sheet, which provides a pathway to close packing with retention of the hydrogen-bond connectivity in the GS network. Moreover, the 2D character of the GS network permits an indefinite number of “projection topologies”—defined by the pattern of “up-down” projections of the organosulfonate groups from the two sides of the GS sheet—which enables the lamellar architectures to accommodate packing of pillars with complex shapes or form inclusion cavities to accommodate a wide range of guest molecules.^{19,20} Furthermore, recent studies have demonstrated the use of organotrissulfonates, tetrasulfonates, and hexasulfonates to form hydrogen-bonded frameworks whose architectures range from tubular^{21,22} to quasi-truncated octahedron cages.²³ More than 500 crystalline compounds comprising a wide range of organosulfonates and guests (in the case of inclusion compounds) with lamellar, cylindrical, and cubic architectures have been synthesized and characterized structurally by our group and others, which is a testament to Peggy’s vision of the role of hydrogen bonding in crystal engineering.

The persistence of the GS network has enabled the synthesis of crystalline compounds wherein function can be introduced through guests included in the framework cavities.^{24–27} For example, para-substituted organodisulfonate pillars have been used recently to control the orientation and aggregation of various guests, ranging from oligothiophenes to laser dyes.^{24,25} The regulation of these attributes can have significant implications for the design of functional materials, including organic light-emitting diodes, field-effect transistors, solar cells, and lasers. Moreover, improved understanding of the structure–function relationships between molecular packing and optoelectronic processes, such as light emission and charge transport, is essential for advances in these arenas. Building on the unique character and robustness of the GS network, we describe herein crystalline materials with new lamellar architectures constructed from ortho-substituted stilbenedisulfonate pillars with “tetris-like” shapes. The stilbene residues adopt densely packed face-to-face brickwork and herringbone motifs that result in strong electronic coupling, as evident from absorption and emission characteristics in the visible region.

EXPERIMENTAL SECTION

Materials and Methods. Preparation of G_2 DSBDS. Stilbene 420 (2,2′-([1,1′-biphenyl]-4,4′-diyl)di-2,1-ethenediyl)bis-benzenesulfonic acid disodium salt, Na_2 DSBDS) was purchased from Exciton Inc. and converted to the acid form by passing it through an Amberlyst 36 ion-exchange column. The acid form was introduced to an aqueous solution (deionized water) containing guanidinium tetrafluoroborate to obtain the guanidinium salt of stilbene 420, G_2 DSBDS. The mixture was then

dried using a rotary evaporator, added to acetone to dissolve any residual guanidinium tetrafluoroborate, and filtered to yield G₂DSBDS as a white powder. Single crystals were grown from a methanol solution saturated with G₂DSBDS by slow evaporation over a period of 4 weeks, resulting in light-yellow color crystals with plate-like morphology bounded by {100}, {010}, and {001} faces (Figure S2).

Preparation of G₂PV3DS. 2,2'-((1*E*,1'*E*)-1,4-phenylenebis(ethene-2,1-diyl))dibenzene sulfonate disodium salt (Na₂PV3DS) was synthesized using a reported procedure²⁸ with slight modifications (see Supporting Information). The product crystallized as yellow plates after recrystallization from hot water. G₂PV3DS was synthesized using the same procedure as described above for G₂DSBDS. Single crystals of G₂PV3DS were grown from a methanol solution saturated with G₂PV3DS by slow evaporation over a period of 3 days, resulting in colorless crystals with plate-like morphology bounded by {101}, {010}, and {101} faces in polymorph I and {100}, {010}, and {101} faces in polymorph II (Figure S2).

Characterization. Single crystal X-ray diffraction data was obtained using a Bruker SMART APEXII diffractometer equipped with a CCD detector. The X-ray beam generated from a sealed Mo tube is monochromated by a graphite crystal and collimated by a 0.5 mm MonoCap collimator. The wavelength from the Mo K α radiation is 0.71073 Å. The crystal temperature (100 K) was controlled by an Oxford Cryosystems 700+ Cooler. Crystals were mounted on a 0.2 mm MicroMount (MiTeGen) with Type B immersion oil (Cargille Labs). Data were collected and processed using the APEX2 software²⁹ for data reduction, data correction, and cell refinement. The structures were solved by SHELXT³⁰ and refined with full-matrix least-squares by SHELXL.³¹ Non-hydrogen atoms were refined with anisotropic displacement parameters, and hydrogen atoms were placed in idealized positions and refined with riding models. The structure refinement of the two polymorphs of G₂PV3DS required fitting with models with approximately 8% disorder. Distance restraints were applied to the disordered components in both structures to fit the idealized geometry. The disorder in both polymorph I (*P*₂/*n*) and polymorph II (*Pca*₂) is the reflection of the main structure about the (010) plane. Powder X-ray diffraction was performed using a Bruker D8 Discover microdiffractometer with the General Area Detector Diffraction System (GADDS) equipped with a VANTEC-2000 2D detector. The X-ray beam was monochromated with a graphite crystal (λ Cu K α = 1.54178 Å) and collimated with a 0.5 mm MonoCap collimator. The data were collected using the GADDS program, merged, and integrated by the XRD2EVAL routine in the Bruker PILOT software.³² The results were employed for Rietveld refinements to determine the phase composition using the software TOPAS 4.2 (Bruker AXS, 2009) with the empirical approach.³³ The standard SRM 660b for powder diffraction (i.e., lanthanum hexaboride (LaB₆)) certified by the National Institute of Standards and Technology (NIST) was used to calculate the empirical instrument function. The resulting instrument function parameters were fixed for the refinement of the powder pattern of the mixture of two G₂PV3DS polymorphs. Refined parameters include background contribution as Chebyshev polynomial of fifth order and 1/*x* function, zero error, sample displacement, scale factor, and lattice parameters. Absorption spectra of the compounds dissolved in methanol were obtained by using UV-vis spectrophotometer (PerkinElmer Inc., LAMBDA 950). Solution-phase and solid-state fluorescence spectra were obtained using a fluorimeter (HORIBA Ltd., FluoroMax-4). For the measurement of single crystal spectra, crystals were mounted on quartz slides using a small amount of immersion oil. Fluorescence spectra were measured in the front face mode using a stage (HORIBA Ltd., 1933 Solid Sample Holder).

RESULTS AND DISCUSSION

The 3-fold symmetry and hydrogen-bond complementarity of the guanidinium cation ($G = (C(NH_2)_3)^+$) and the sulfonate moieties of organodisulfonate anions (DS; $S = -O_3S-R-SO_3^-$) typically affords a 2D quasi-hexagonal hydrogen-bonding network, with the organodisulfonate serving as a pillar that

bridges opposing GS sheets as a consequence of the opposite orientation of the sulfonate groups along a single axis (Figure 1). Typically, the sulfur–sulfur distance along the major GS ribbon axis (*a*₁) is 7.5 ± 0.2 Å along the *a*₁ axis, but it ranges from 7.0 to 13.0 Å along the *b*₁ axis, depending on the puckering angle of GS sheets (θ , Figure 1B). In the case of typical organodisulfonate pillars, the length of the pillar, with its long axis nominally perpendicular to the GS sheets, determines the distance between opposing GS sheets, whereas guest molecules, incorporated into the cavities supported by the pillar, play an important role in regulating the framework architecture and projection topologies of the pillars.^{16,19,24,25}

In the case of ortho-substituted disulfonates, such as the stilbene disulfonates PV3DS²⁻ and DSBDS²⁻, the only possible orientation of the pillar would be with its long axis parallel to the GS sheet. A discrete bilayer architecture, in which the two sulfonate groups of each pillar attach to the same side of a GS sheet (i.e., a *Z* configuration with respect to the alignment of the sulfonate groups), is unlikely because the sulfonate–sulfonate distance of pillar would need to be commensurate with the sulfonate nodes in a single GS sheet. Conversely, a pillar can connect opposing GS sheets (i.e., a *E* configuration) in a continuously layered architecture because this distance criterion is relaxed, requiring only planar PV3 and DSB moieties and registry of the opposing sheets in a manner that avoids steric interference between neighboring pillars. Molecular models based on the lengths of the PV3DS²⁻ and DSBDS²⁻ pillars ($L_{PV3DS} = 20.02$ Å and $L_{DSBDS} = 24.23$ Å, including van der Waals radii) and the possible projection topologies of the sulfonate nodes in a continuously layered architecture (i.e., whether the sulfonate nodes project “up” or “down” from the GS sheet) suggest that these pillars can pack with their long axes diagonal to the GS major ribbon axis, along a vector defined by two sulfonate nodes in adjacent ribbons on a GS sheet, separated by a distance $d = 13.0 \pm 0.2$ Å (Figure 1, Figure S1). In this manner, the long tetris-shaped pillar traverses a void region created by a sulfonate node in a “down” projection. The pillars must organize in a manner that maximizes their packing density, particularly if guest inclusion is to be avoided.

Slow evaporation of methanol solutions containing G₂DSBDS afforded light-yellow colored crystals with plate-like morphology of guest-free G₂DSBDS. Faster evaporation produced needle-like crystals on the order of 10 μ m in one axis that were unsuitable for single crystal X-ray diffraction. Single crystal X-ray diffraction reveals that G₂DSBDS crystallized in the monoclinic *P*₂/*c* space group ($a = 21.1455(19)$ Å, $b = 12.7188(12)$ Å, $c = 17.8085(16)$ Å, $\beta = 105.0780(16)^\circ$, $V = 4624.62(7)$ Å³). The sulfonate groups, on the opposite ends of DSB, connect two opposing quasi-hexagonal GS sheets with the long axis of the stilbene pillars parallel to the GS sheets (Figure 2). Consequently, the distance between the GS sheets is governed by the short axis of DSBDS²⁻ rather than its length. The framework adopts a continuously layered architecture, in which the GS sheets are continuously connected by the DSBDS²⁻ pillars. The DSB residues occupy a substantial volume fraction between the GS sheets, precluding the incorporation of guest molecules. Interestingly, distance between the sulfonate nodes along the major ribbon (*a* axis) is not uniform, repeating as $\dots 7.557, 7.130, 6.812$ Å \dots (Figure S3) and resulting in a large unit cell. The 6.812 Å distance is among the shortest observed for GS crystals.

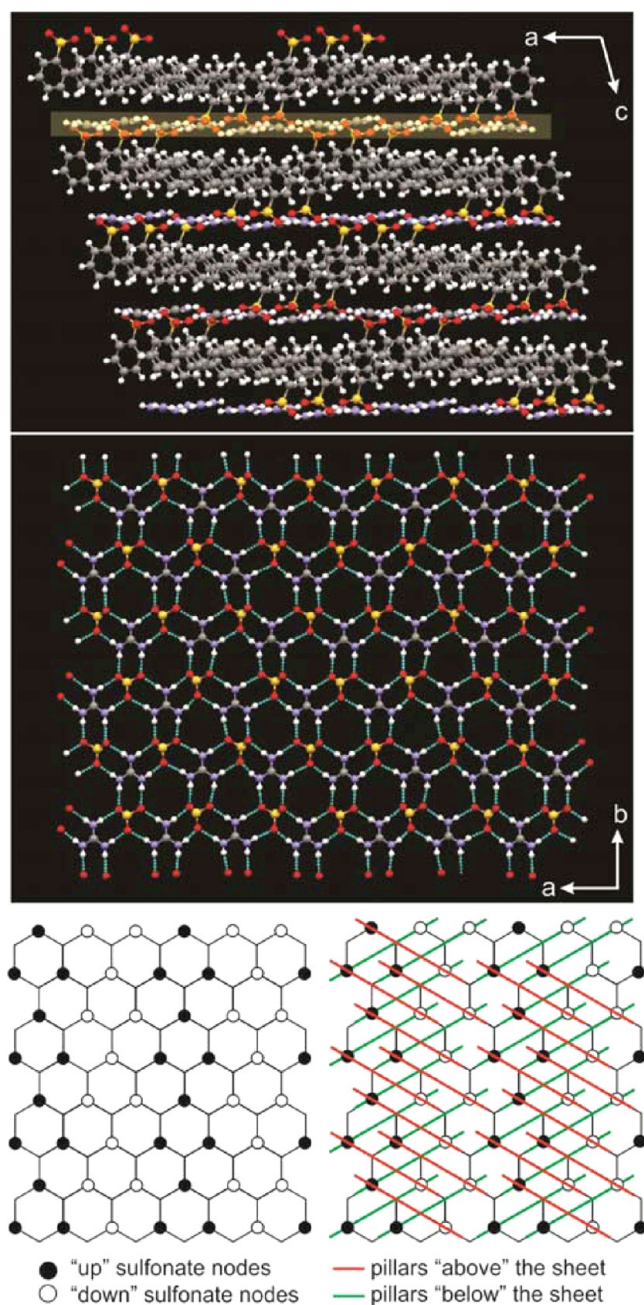


Figure 2. (Top) Crystal structure of G_2 DSBDS as viewed along the b -axis, illustrating the lamellar structure with the continuously layered architecture. One of the GS sheets is shaded yellow. (Middle) The quasi-hexagonal hydrogen-bonded GS sheet in G_2 DSBDS, with the DSB residues removed for clarity. (Bottom, left) Filled and open circles denote "up" and "down" projections of the sulfonate nodes from surface of the GS sheet, respectively. (Bottom, right) In-plane alignment of the DSB pillars above (red line) and below (green line) each GS sheet. The DSB moieties above (red) traverse voids created by the "down" projections of the sulfonate nodes on the same sheet (open circles).

The projection topology of the GS sheet in G_2 DSBDS can be used to describe the pattern of the sulfonate nodes with respect to their "up" and "down" projections, denoted as filled and open circles, respectively (Figure 2, bottom). This projection topology differs from the previously observed examples, which have been denoted as discrete bilayer, simple brick, zigzag brick, and double brick (Figure S1). The red and green lines in Figure

2 denote the orientation of the DSB moieties above and below each GS sheet, respectively. Unlike the previously reported topologies, G_2 DSBDS adopts a configuration in which one-half of the major GS ribbons adopt an ...up, down, down... sequence and the other half a ...down, down, up... sequence. Although not observed previously, this configuration was predicted as one of the possible architectures.³⁴

The effect of pillar length on the packing motif ($L_{PV3DS} = 20.02 \text{ \AA}$ vs $L_{DSBDS} = 24.23 \text{ \AA}$) was evident from the single crystal structures of two polymorphs of G_2 PV3DS, also crystallized by slow evaporation of methanol to produce colorless crystals with a plate-like habit. Polymorph I exhibits a monoclinic $P2_1/n$ space group ($a = 19.603(3) \text{ \AA}$, $b = 7.6017(10) \text{ \AA}$, $c = 19.639(3) \text{ \AA}$, $\beta = 112.7510(17)^\circ$, $V = 2698.83(6) \text{ \AA}^3$). Polymorph II crystallizes in the orthorhombic $Pca2_1$ space group ($a = 21.7900(10) \text{ \AA}$, $b = 7.5850(3) \text{ \AA}$, $c = 16.3519(7) \text{ \AA}$, $V = 2702.6(2) \text{ \AA}^3$). Comparison of the structures of the two polymorphs (Figures 3 and 4) suggests similar molecular packing and molecular conformations, which can be discerned by superimposing the motifs of the GS sheets and the PV3 packing of both forms (Figure S4). The simulated and experimental powder X-ray diffraction patterns from each structure differ only with respect to three unique reflections (Figure S5 and S6). Both polymorphs reveal a guest-free lamellar structure and a continuously layered architecture in which the PV3 moieties are confined between the GS sheets. The GS sheets adopt the quasi-hexagonal hydrogen-bonded network. In contrast to G_2 DSBDS, the GS sheets in both polymorphs of G_2 PV3DS are puckered with the angle of $\theta \approx 130^\circ$. This can be explained by the smaller volume of PV3 compared to DSB; puckering of the GS sheets enables the smaller PV3 moieties to achieve the dense packing required for crystallization, illustrating the important role of compliance in the GS sheet. Both polymorphs of G_2 PV3DS adopt the previously reported "simple brick" framework architecture, differing from the new architecture found in G_2 DSBDS. The packing motif of the PV3 moieties also differs significantly compared with DSBDS, packing in a herringbone pattern rather than the parallel brickwork packing observed for the DSB moieties in G_2 DSBDS.

As predicted, the DSB and PV3 residues in all three structures are oriented along an axis that traverses the direction defined by two sulfonate nodes in adjacent ribbons, along the diagonal direction that spans a distance $d = 13.0 \pm 0.2 \text{ \AA}$ in the idealized flat GS sheet. In the continuously layered architecture, the pillar thereby is situated in a void space created by a "down" projection of a sulfonate node, despite the difference in the length of the DSB and PV3 residues. This observation illustrates once again the compliance of GS networks, which can adopt different framework architectures and pucker (in the simple brick form) to accommodate a substantial difference in the length and molecular volume of the residues. Moreover, preliminary calculations of the optimized gas-phase geometries using the COMPASS force field predict nearly planar geometries for the PV3 and DSB moieties—either alone or decorated with sulfonate groups or various neutral substituents at the ortho positions—compatible with the requirements for stacking of these moieties between the GS sheets (substantial deviations from planarity are predicted only for larger substituents such as *t*-butyl, as would be expected). The formation of the continuously layered architecture requires that the two ortho sulfonate groups project to opposite sides of the PV3 and DSB moieties (the *E* configuration). Calculations with

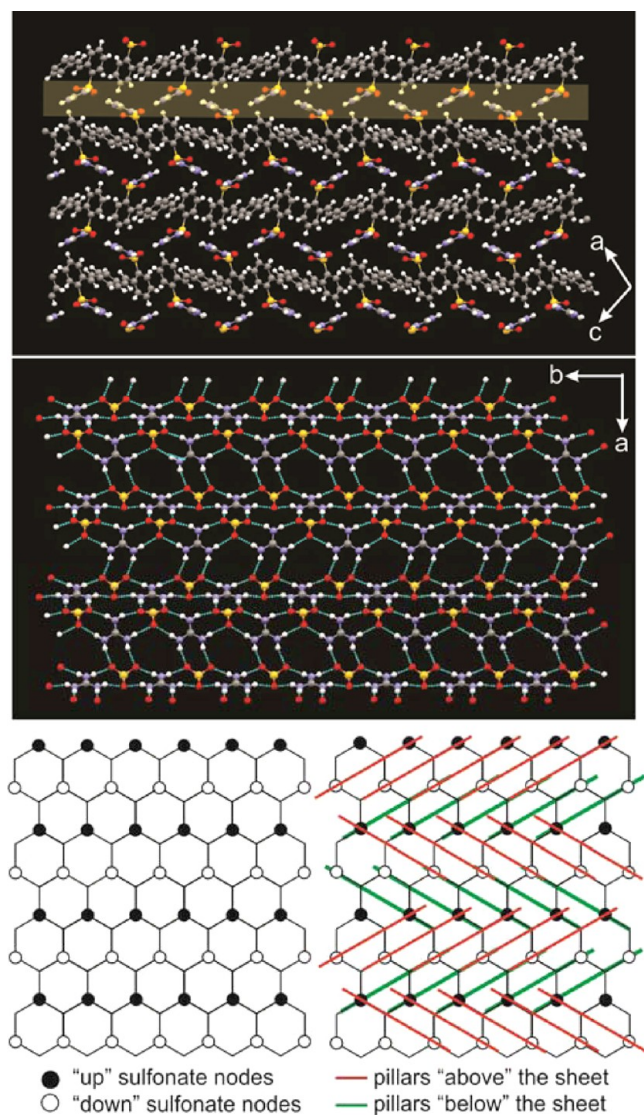


Figure 3. (Top) Crystal structure of G_2PV3DS polymorph I ($P2_1/n$) viewed along the b -axis, illustrating the lamellar structure with the continuously layered architecture. One of the GS sheets is shaded yellow. (Middle) The quasi-hexagonal hydrogen-bonded GS sheet in G_2PV3DS polymorph I, with the PV3 residues removed for clarity. (Bottom, left) Filled and open circles denote “up” and “down” projections of the sulfonate nodes from surface of the GS sheet, respectively. (Bottom, right) In-plane alignment of the PV3 pillars above (red line) and below (green line) each GS sheet. The PV3 moieties above the sheet (red) traverse voids created by the “down” projections of the sulfonate nodes on the same sheet (open circles).

the COMPASS force field to determine the preference for either an E or Z configuration were equivocal for the compounds in this group, however (Tables S1 and S2, Figure S8). Moreover, the calculations suggested that the Z configuration was favored for DSBDS (by 8 kcal/mol), but the E configuration was favored for PV3DS (by 40 kcal/mol) (Figure S8). The energy differences between these configurations for the neutral substituents are in the range $3 \leq \Delta E$ (kcal/mol) ≤ 10 . Although the energy difference between the configurations of PV3DS seems anomalously large (ca. 80 kT) and warrants further investigation with more rigorous methods, these calculations suggest that the energy difference between the E and Z configurations are sufficiently small for packing

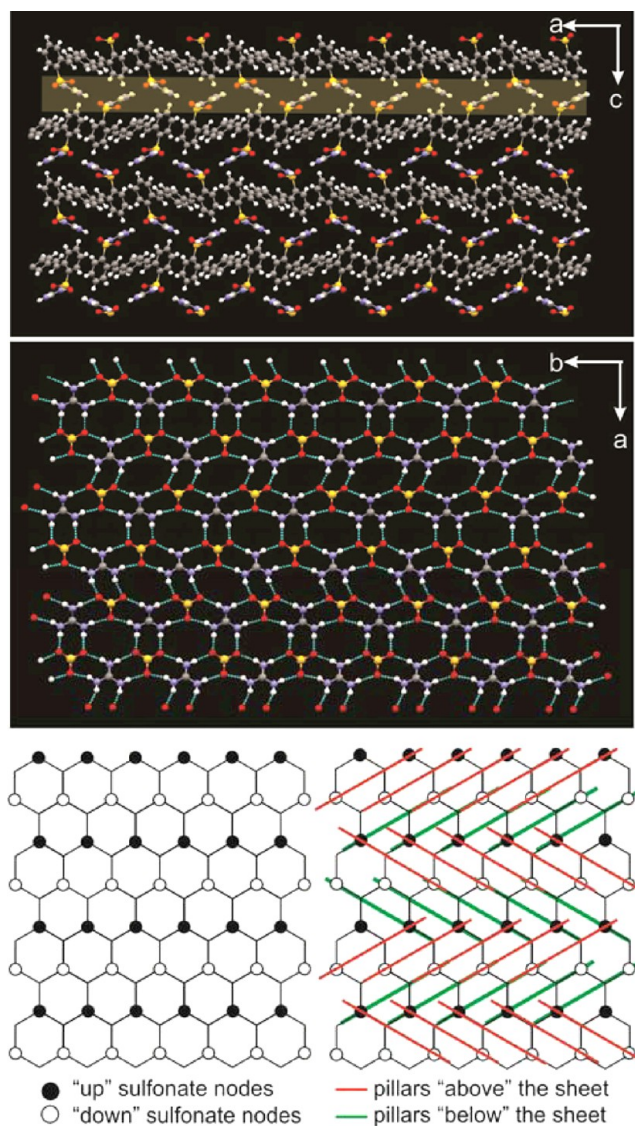


Figure 4. (Top) Crystal structure of G_2PV3DS polymorph II ($Pca2_1$) viewed along the b -axis, illustrating the lamellar structure with the continuously layered architecture. One of the GS sheets is shaded yellow. (Middle) The quasi-hexagonal hydrogen-bonded GS sheet in G_2PV3DS polymorph II, with the PV3 residues removed for clarity. (Bottom, left) Filled and open circles denote “up” and “down” projections of the sulfonate nodes from surface of the GS sheet, respectively. (Bottom, right) In-plane alignment of the PV3 pillars above (red line) and below (green line) each GS sheet. The PV3 moieties above the sheet (red) traverse voids created by the “down” projections of the sulfonate nodes on the same sheet (open circles).

forces to readily overcome a preference for either isomer, enabling ready formation of a framework with the pillars in the E configuration.

The dense packing of the DSB and PV3 residues confined between the GS sheets precludes the incorporation of guest molecules, allowing strong intermolecular electronic couplings between the stilbene-like fragments. G_2DSBDS adopts a brickwork packing motif (Figure 5A,B) in which a face-to-edge association of the DSB residues is prohibited by the orientation of the sulfonate groups enforced by the parallel GS sheet. Consequently, the DSB residues pack in a face-to-face configuration. J-aggregates are thought to adopt similar brickwork motifs in solution, accompanied by bathochromic

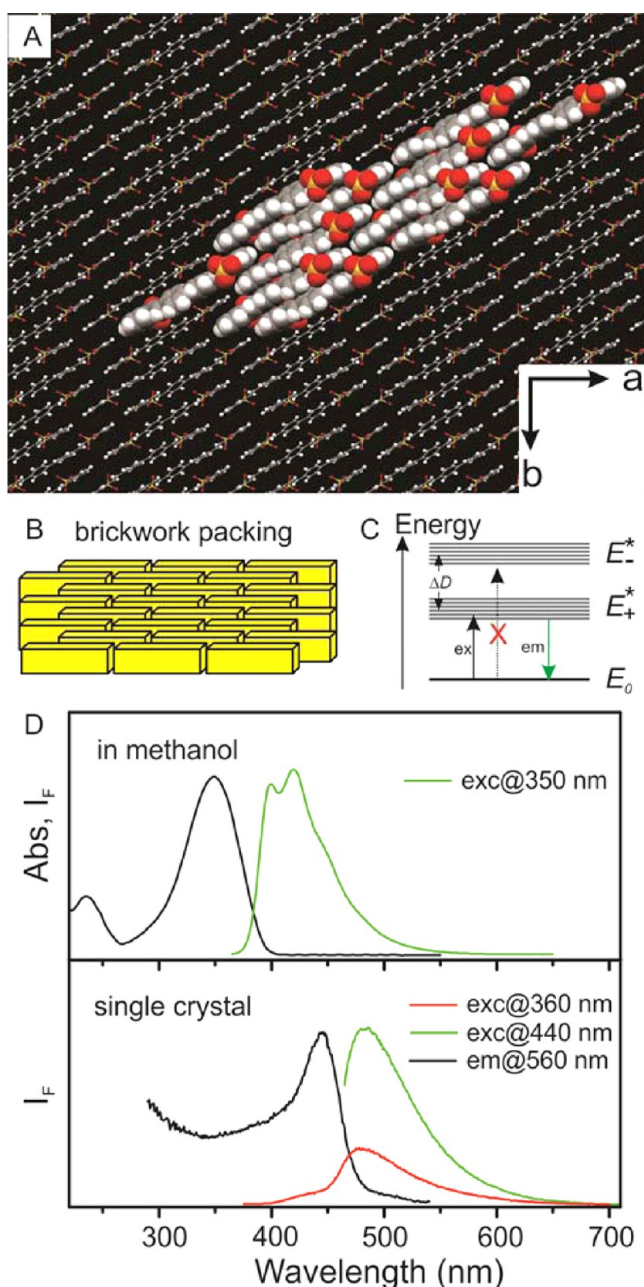


Figure 5. (A) Packing of DSBDS pillars viewed down the c -axis, with 11 molecules depicted as space filling and the rest as wireframe. Guanidinium ions are omitted for clarity. (B) Schematic representation of brickwork packing. (C) A simplified energy diagram for the brickwork packing motif denoting the allowed and disallowed transitions. ΔD is Davydov splitting. (D) Absorbance (black) and fluorescence (green) spectra of DSBDS in methanol and fluorescence and excitation spectrum of a G_2 DSBDS crystal. The broad excitation spectrum at wavelengths below the peak at 445 nm suggests transitions to a broad dispersion of excited states.

shifts of the absorbance and emission spectra with respect to their corresponding monomer forms.³⁵ G_2 DSBDS also exhibits large bathochromic shifts of both absorbance ($\Delta\lambda = 95$ nm, $\Delta E = -0.76$ eV) and fluorescence ($\Delta\lambda = 86$ nm, $\Delta E = -0.55$ eV) compared with monomeric DSBDS²⁻ in methanol solution (Figure 5D; the absorbance and fluorescence peaks in methanol are 350 and 400 nm, respectively). It is well established that the formation of dye molecule aggregates results in a splitting of the

excited electronic states (i.e., Davydov splitting). In the case of J-aggregates the electronic transition from the ground state (E_0) to the lower electronic excited band (E_+^*) is allowed, whereas the transition from E_0 to the higher electronic excited band (E_-^*) is forbidden due to the cancellation of transition dipoles (Figure 5C). The bathochromic shifts observed for G_2 DSBDS are therefore consistent with an electronic structure resembling that expected for J-aggregates. The $E_0 \rightarrow E_-^*$ transition is forbidden in the brickwork packing because the offset along the long molecular axes of neighboring molecules cancels (or nearly so) the transition dipoles in the E_-^* state. The observed Stokes shift (the peak difference between absorbance and fluorescence spectrum) in G_2 DSBDS ($\Delta\lambda = 41$ nm, $\Delta E = -0.24$ eV) was less than that observed in solution ($\Delta\lambda = 50$ nm, $\Delta E = -0.44$ eV), and the vibronic structure of the spectrum was observed only in solution. Collectively, these features are consistent with strong J-type intermolecular electronic coupling. The excitation spectrum for the emission peak at 486 nm extends down to 300 nm. The observation of spectral bands that are much broader than those of J-aggregates in solution³⁵ suggests a broad dispersion of excited states (E_+^* and E_-^*) in the solid state and relaxation of the selection rules for the optical transition.

In contrast to G_2 DSBDS, the PV3 residues in G_2 PV3DS stack face-to-face in a herringbone motif (Figure 6A,B). This arrangement affords both hypsochromic and bathochromic shifts in the absorption spectrum relative to the spectrum in methanol. The absorption peak of PV3DS in methanol appears at 352 nm, while peaks at 313 and 423 nm were observed for G_2 PV3DS (Figure 6D). This is consistent with electronic transitions from the ground state (E_0) to both the lower (E_+^*) and higher electronic excited states (E_-^*) (Figure 6C).³⁶ The observation of both bathochromic and hypsochromic shifts ($\Delta\lambda = 71$ nm, $\Delta E = -0.59$ eV; $\Delta\lambda = -39$ nm, $\Delta E = 0.44$ eV) indicates that the higher energy transition is no longer forbidden as with the brickwork aggregates in G_2 DSBDS, such that both the $E_0 \rightarrow E_+^*$ and $E_0 \rightarrow E_-^*$ transitions are allowed as expected for a herringbone arrangement, in which there is a nonzero vector sum of the transition dipoles in both states. The magnitude of the Davydov splitting, which is a measure of the strength of electronic coupling, is $\Delta D = 1.03$ eV, significantly larger than typical values for simple polyacene crystals that pack in a face-to-edge herringbone motif (ΔD (anthracene) = 25 meV and ΔD (naphthalene) = 19 meV).³⁶ This indicates that the GS framework enforces a strong intermolecular electronic coupling of the *face-to-face* PV3 residues.^{37,38} The emission in the solid state occurs only from the E_+^* state due to efficient intraband relaxation. Notably, the spectra for both polymorphs of G_2 PV3DS were identical, reflecting the nearly identical conformations and packing of the pillars between the GS sheets. Moreover, the spectral bands were too broad to observe individual contributions from the different conformers in both G_2 DSBDS and G_2 PV3DS crystals, which may be distinguishable only at ultralow temperatures.

CONCLUSION

Lamellar guanidinium organodisulfonate (GDS) hydrogen-bonded frameworks constructed from tetris-shaped ortho-substituted disulfonates of stilbene derivatives display crystal architectures in which the disulfonates serve as pillars that connect opposing guanidinium sulfonate (GS) sheets while guiding the organization of the stilbene components into packing motifs that produce unique optical properties. The G_2 DSBDS and G_2 PV3DS frameworks form lamellar continu-

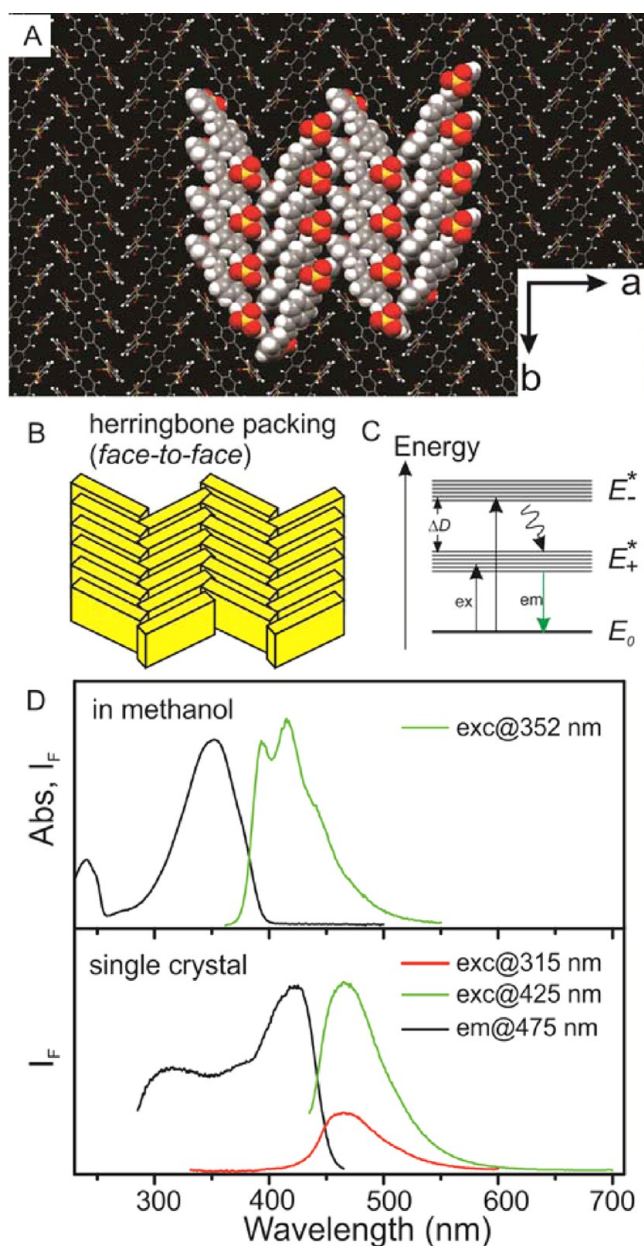


Figure 6. (A) Packing of PV3DS pillars viewed down the *c*-axis, with 16 molecules depicted as space filling and the rest as wireframe, illustrated here for the $Pna2_1$ polymorph. Guanidinium ions are omitted for clarity. (B) Schematic of face-to-face herringbone packing. (C) A simplified energy diagram for the face-to-face herringbone packing motif with transition pathway depicted with arrows. A wavy arrow represents phonon relaxation and ΔD is Davydov splitting. (D) Absorbance (black) and fluorescence (green) spectra of PV3DS in methanol solution, and fluorescence and excitation spectrum of a G_2 PV3DS crystal. The broad excitation spectrum at wavelengths between the peak at 313 and 423 nm suggests transitions to a broad dispersion of excited states.

ously layered architectures with dense packing of the tetris-shaped pillars while maintaining the 2D quasi-hexagonal structure of the GS networks. The puckering of the GS sheet in the two polymorphs of G_2 PV3DS reveals the unique structural compliance of the 2D GS network, in these cases accommodating pillars of different lengths that traverse void spaces created between the GS sheets owing to the continuously layered architecture. The observation of these

compounds and consideration of other sulfonate projection topologies suggest that GS compounds with even longer transverse pillars may be achievable through enforced confinement between the GS sheets (Figure 7), although these

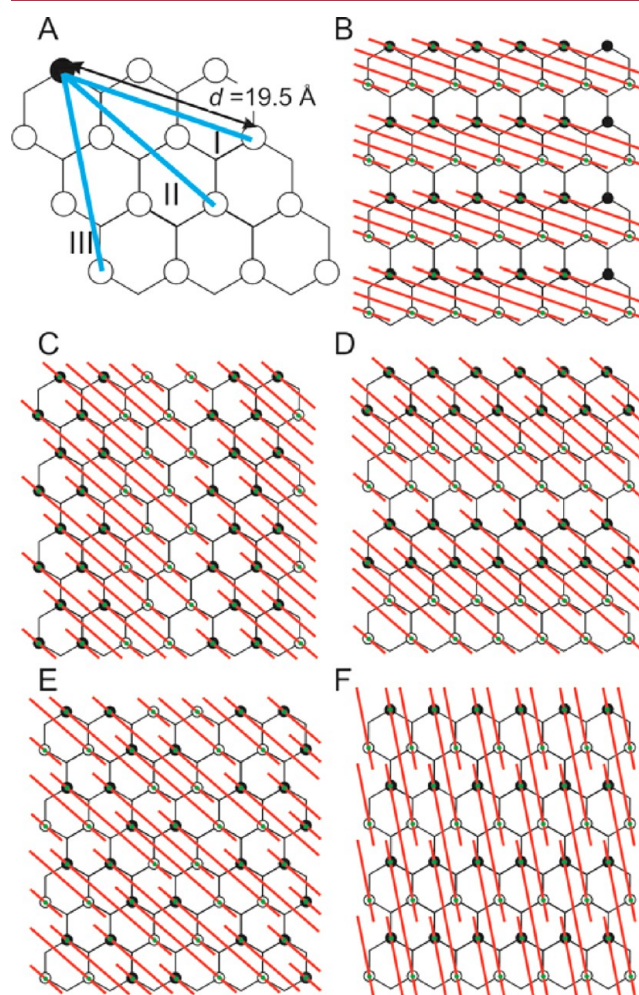


Figure 7. Prospective GS sheet projection topologies for long tetris-shaped pillars. (A) The blue solid lines represent three possible alignments of the long axis of the tetris-shaped pillars on the flat GS sheet. (B–F) Five examples of the in-plane alignment of the organosulfonate residues pillars that satisfy the constraint of steric avoidance.

candidates require different alignments of the organic residues with respect to the major GS ribbon. As exemplified by G_2 DSBDS and G_2 PV3DS, unique optical properties due to strong intermolecular electronic coupling can be achieved by certain confined packing motifs. Elucidation of key structure–property relationships, including optical properties^{39,40} and charge mobility,^{1,2,38} can be facilitated by structural enforcement like that provided by the GS frameworks. For example, brickwork packing like that observed in G_2 DSBDS has been suggested as preferable for high charge mobility compared with herringbone packing,^{41–43} although this postulate has not been fully tested.⁴⁴ Notably, rubrene forms face-to-face herringbone packing, but its charge mobility is quite large.^{2,45} The compounds described above and the persistence of the GS sheet suggest a path forward to examine electronic coupling between chromophores in a systematic manner using the

versatility of organic synthesis to generate various disulfonated chromophores.

■ ASSOCIATED CONTENT

● Supporting Information

Synthesis and ^1H NMR spectra of G_2DSBDS and $\text{G}_2\text{PV3DS}$, simulated and experimental powder X-ray diffraction data of $\text{G}_2\text{PV3DS}$, details of COMPASS force field simulations, crystallographic data in CIF format. The Supporting Information is available free of charge on the ACS Publications website at DOI: 10.1021/acs.cgd.5b00452.

■ AUTHOR INFORMATION

Corresponding Author

*E-mail: mdw3@nyu.edu.

Notes

The authors declare no competing financial interest.

■ ACKNOWLEDGMENTS

The authors acknowledge the support of the National Science Foundation through DMR-1308677, the NSF CRIF Program (CHE-0840277), and the NSF MRSEC Program (DMR-0820341) for shared facilities. T.A. thanks the JSPS Postdoctoral Fellowships for Research Abroad for the financial support.

■ REFERENCES

- (1) Anthony, J. E. *Chem. Rev.* **2006**, *106*, 5028–5048.
- (2) Wang, C. L.; Dong, H. L.; Hu, W. P.; Liu, Y. Q.; Zhu, D. B. *Chem. Rev.* **2012**, *112*, 2208–2267.
- (3) Etter, M. C.; MacDonald, J. C.; Bernstein, J. *Acta Crystallogr., Sect. B* **1990**, *46*, 256–262.
- (4) Etter, M. C. *Acc. Chem. Res.* **1990**, *23*, 120–126.
- (5) The special issue of: Hollingsworth, M. D.; Ward, M. D. *Structure and Chemistry of the Organic Solid State. Chem. Mater.* **1994**, *6*, 1087–1461.
- (6) Ward, M. D. *Chem. Commun.* **2005**, 5838–5842.
- (7) Gilli, P.; Bertolasi, V.; Ferretti, V.; Gilli, G. *J. Am. Chem. Soc.* **1994**, *116*, 909–915.
- (8) Taylor, R.; Kennard, O. *Acc. Chem. Res.* **1984**, *17*, 320–326.
- (9) Speakman, J. C. Acid salts of carboxylic acids, crystals with some “very short” hydrogen bonds. In *Structure and Bonding*; Springer: Berlin, 1972; Vol. 12, pp 141–199.
- (10) Hosseini, M. W. *Acc. Chem. Res.* **2005**, *38*, 313–323.
- (11) Dalrymple, S. A.; Shimizu, G. K. H. *J. Am. Chem. Soc.* **2007**, *129*, 12114–12116.
- (12) Dalrymple, S. A.; Shimizu, G. K. H. *Chem. Commun.* **2006**, 956–958.
- (13) Wang, X.-Y.; Sevov, S. C. *Chem. Mater.* **2007**, *19*, 4906–4912.
- (14) Russell, V. A.; Etter, M. C.; Ward, M. D. *J. Am. Chem. Soc.* **1994**, *116*, 1941–1952.
- (15) Russell, V. A.; Etter, M. C.; Ward, M. D. *Chem. Mater.* **1994**, *6*, 1206–1217.
- (16) Holman, K. T.; Pivovar, A. M.; Swift, J. A.; Ward, M. D. *Acc. Chem. Res.* **2001**, *34*, 107–118.
- (17) Burke, N. J.; Burrows, A. D.; Mahon, M. F.; Teat, S. J. *CrystEngComm* **2004**, *6*, 429–436.
- (18) Dumitrescu, D.; Legrand, Y.-M.; Dumitrescu, F.; Barboiu, M.; van der Lee, A. *Cryst. Growth Des.* **2012**, *12*, 4258–4263.
- (19) Russell, V. A.; Evans, C. C.; Li, W. J.; Ward, M. D. *Science* **1997**, *276*, 575–579.
- (20) Swift, J. A.; Reynolds, A. M.; Ward, M. D. *Chem. Mater.* **1998**, *10*, 4159–4168.
- (21) Xiao, W.; Hu, C.; Ward, M. D. *J. Am. Chem. Soc.* **2014**, *136*, 14200–14206.
- (22) Liu, Y.; Xiao, W.; Yi, J. J.; Hu, C.; Park, S.-J.; Ward, M. D. *J. Am. Chem. Soc.* **2015**, *137*, 3386–3392.
- (23) Liu, Y. Z.; Hu, C. H.; Comotti, A.; Ward, M. D. *Science* **2011**, *333*, 436–440.
- (24) Soegiarto, A. C.; Ward, M. D. *Cryst. Growth Des.* **2009**, *9*, 3803–3815.
- (25) Soegiarto, A. C.; Comotti, A.; Ward, M. D. *J. Am. Chem. Soc.* **2010**, *132*, 14603–14616.
- (26) Soegiarto, A. C.; Yan, W.; Kent, A. D.; Ward, M. D. *J. Mater. Chem.* **2011**, *21*, 2204–2219.
- (27) Xiao, W.; Hu, C.; Ward, M. D. *Cryst. Growth Des.* **2013**, *13*, 3197–3200.
- (28) Soo, H. S.; Agiral, A.; Bachmeier, A.; Frei, H. *J. Am. Chem. Soc.* **2012**, *134*, 17104–17116.
- (29) APEX2 (version 2013.12). Program for Bruker CCD X-ray Diffractometer Control; Bruker AXS Inc.: Madison, WI, 2013.
- (30) Sheldrick, G. M. *SHELXT. Program for Solving Small Molecule Structures, Determining the Space Group and Structure Together*; Universität Göttingen, Göttingen, Germany, 2014.
- (31) Sheldrick, G. M. *SHELXL. Program for Refinement of Crystal Structures*; Universität Göttingen: Göttingen, Germany, 2014.
- (32) GADDS (version 4.1.36) and PILOT (version 2009.4–0). Programs for Bruker CCD X-ray Diffractometer Control; Bruker AXS Inc.: Madison, WI, 2009.
- (33) TOPAS (version 4.2). Software Package for Structure Analysis of Powder Data, Bruker AXS Inc.: Madison, WI, 2009.
- (34) Holman, K. T.; Martin, S. M.; Parker, D. P.; Ward, M. D. *J. Am. Chem. Soc.* **2001**, *123*, 4421–4431.
- (35) Würthner, F.; Kaiser, T. E.; Saha-Möller, C. R. *Angew. Chem., Int. Ed.* **2011**, *50*, 3376–3410.
- (36) Schwoerer, M.; Wolf, H. C. Electronic Excited States, Excitons, Energy Transfer. In *Organic Molecular Solids*; Wiley-VCH Verlag GmbH: New York, 2008; pp 125–175.
- (37) Yavuz, I.; Martin, B. N.; Park, J.; Houk, K. N. *J. Am. Chem. Soc.* **2015**, *137*, 2856–2866.
- (38) Mas-Torrent, M.; Rovira, C. Crystal Structure Performance Relationship in OFETs. In *Functional Supramolecular Architectures*; WILEY-VCH Verlag & Co. KGaA: New York, 2011; pp 649–682.
- (39) Kabe, R.; Nakanotani, H.; Sakanoue, T.; Yahiro, M.; Adachi, C. *Adv. Mater.* **2009**, *21*, 4034–4038.
- (40) Varghese, S.; Park, S. K.; Casado, S.; Fischer, R. C.; Resel, R.; Milián-Medina, B.; Wannemacher, R.; Park, S. Y.; Gierschner, J. *J. Phys. Chem. Lett.* **2013**, *4*, 1597–1602.
- (41) Ando, S.; Murakami, R.; Nishida, J.-i.; Tada, H.; Inoue, Y.; Tokito, S.; Yamashita, Y. *J. Am. Chem. Soc.* **2005**, *127*, 14996–14997.
- (42) Moon, H.; Zeis, R.; Borkent, E.-J.; Besnard, C.; Lovinger, A. J.; Siegrist, T.; Kloc, C.; Bao, Z. *J. Am. Chem. Soc.* **2004**, *126*, 15322–15323.
- (43) Reese, C.; Roberts, M. E.; Parkin, S. R.; Bao, Z. *Adv. Mater.* **2009**, *21*, 3678–3681.
- (44) Hutchison, G. R.; Ratner, M. A.; Marks, T. J. *J. Am. Chem. Soc.* **2005**, *127*, 16866–16881.
- (45) Zeis, R.; Besnard, C.; Siegrist, T.; Schlockermann, C.; Chi, X.; Kloc, C. *Chem. Mater.* **2006**, *18*, 244–248.